Supplementary Figures:

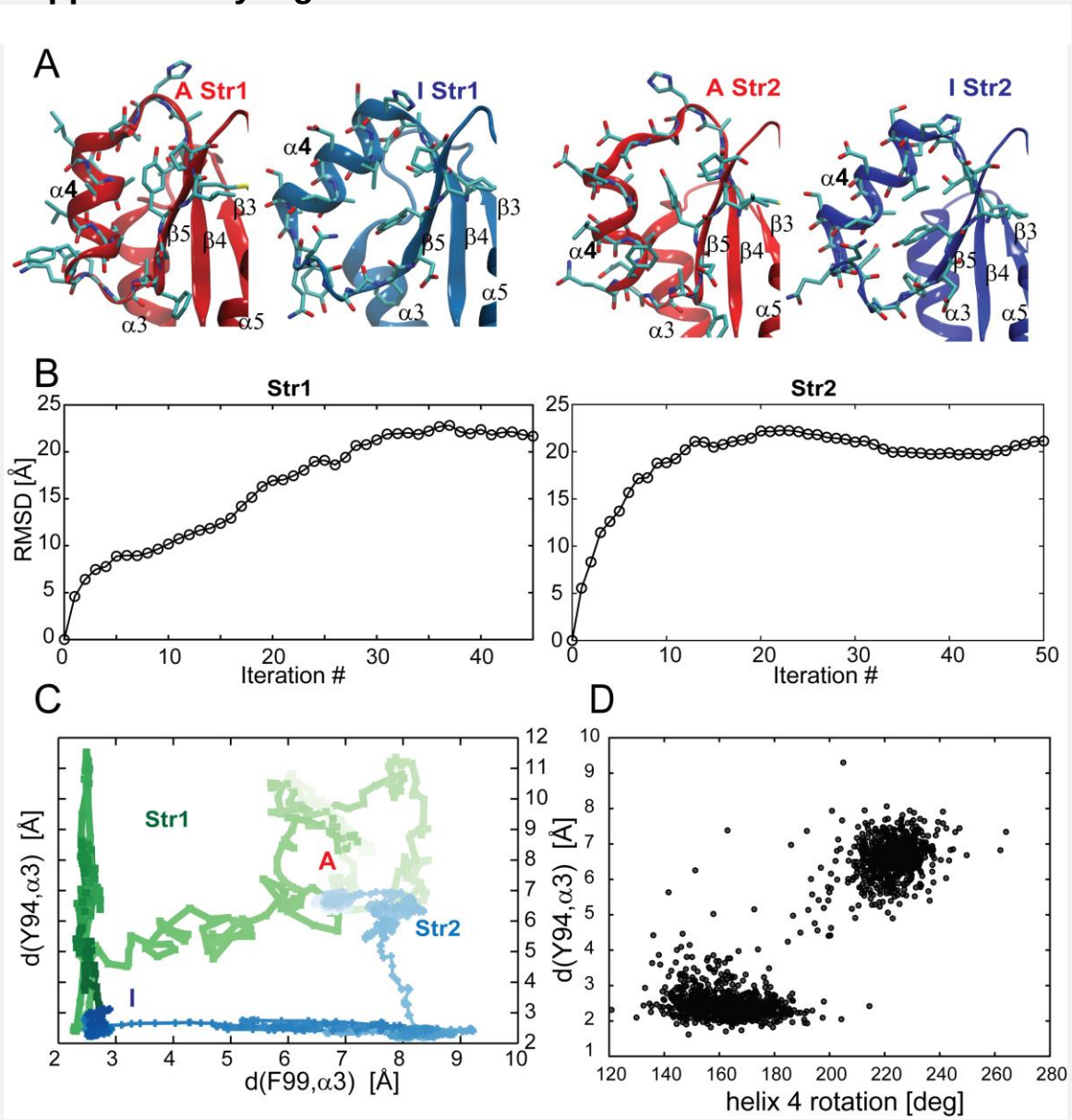

Supplementary Figure 1: The two strings converge to two qualitatively different pathways. **A)** Models of active (red) and inactive (blue) states used as end points for the string calculations in strings Str1 and Str2. **B)** The RMSD of the pathway with respect to the initial reference string as a function of the number of iteration is used as a criterion of convergence of the iterative procedure. **C)** The pathways Str1 and Str2 do not converge to the same pathway, as can be seen from the values of some collective coordinates along the two pathways. **D)** The position of Y94 with respect to helix α3 in Str2 is correlated to the angle of rotation of the helix around its axis.

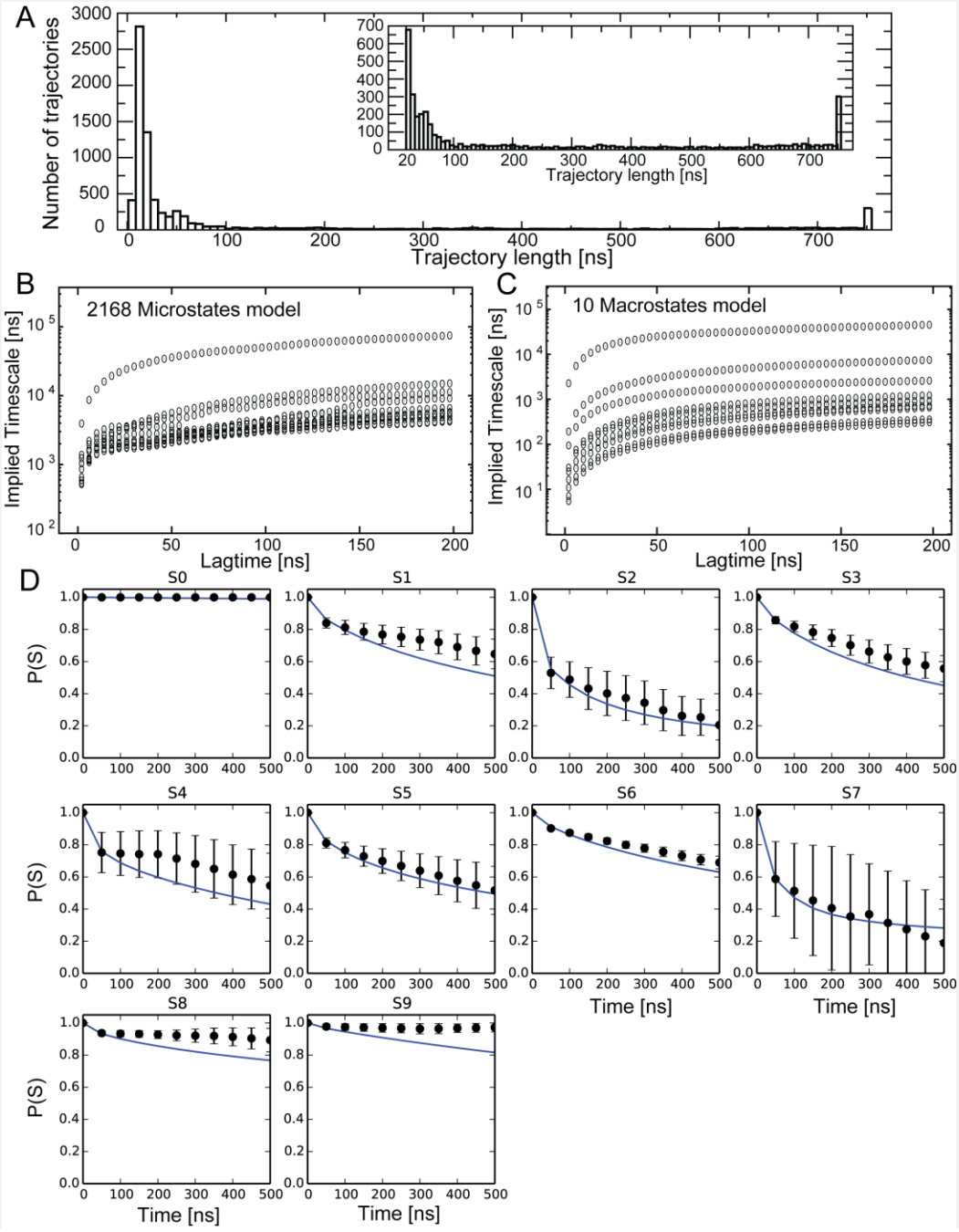

Supplementary Figure 2: Relaxation Timescales and evaluation of the MSM analysis.
A) Distribution of the length of the trajectories sampled during the simulations performed on the F@H distributed computing grid. In the inset the same distribution is shown only for trajectories longer than 20ns.
B,C) Implied relaxation timescales as function of the lagtime Δt. **B)** Implied timescales are obtained from the spectral analysis of the transition probability matrix built by counting the transitions among the 2168 microstates. The transition matrix is built for several lagtimes between 1 ns and 200 ns, and for each lagtime the implied timescales are plotted. The convergence of the slowest modes is achieved for Δt = 50 ns. Consequently a 50 ns lagtime was used for building the MSM. **(C).** The same analysis is repeated after lumping the states in 10 macrostates with the PCCA method[1, 2, 3]. **D)** Chapman-Kolmogorov test[4, 5] to assess the validity of the macrostate

model. For each of the 10 macrostates in our model we initialize the population in that state and compare the evolution of the population predicted from the MSM (solid lines) to that measured on the trajectories (circles). The error bars represent the s.d., estimated with bootstrap of the data repeating the analysis 10 times, each time using only 75% of the available data.

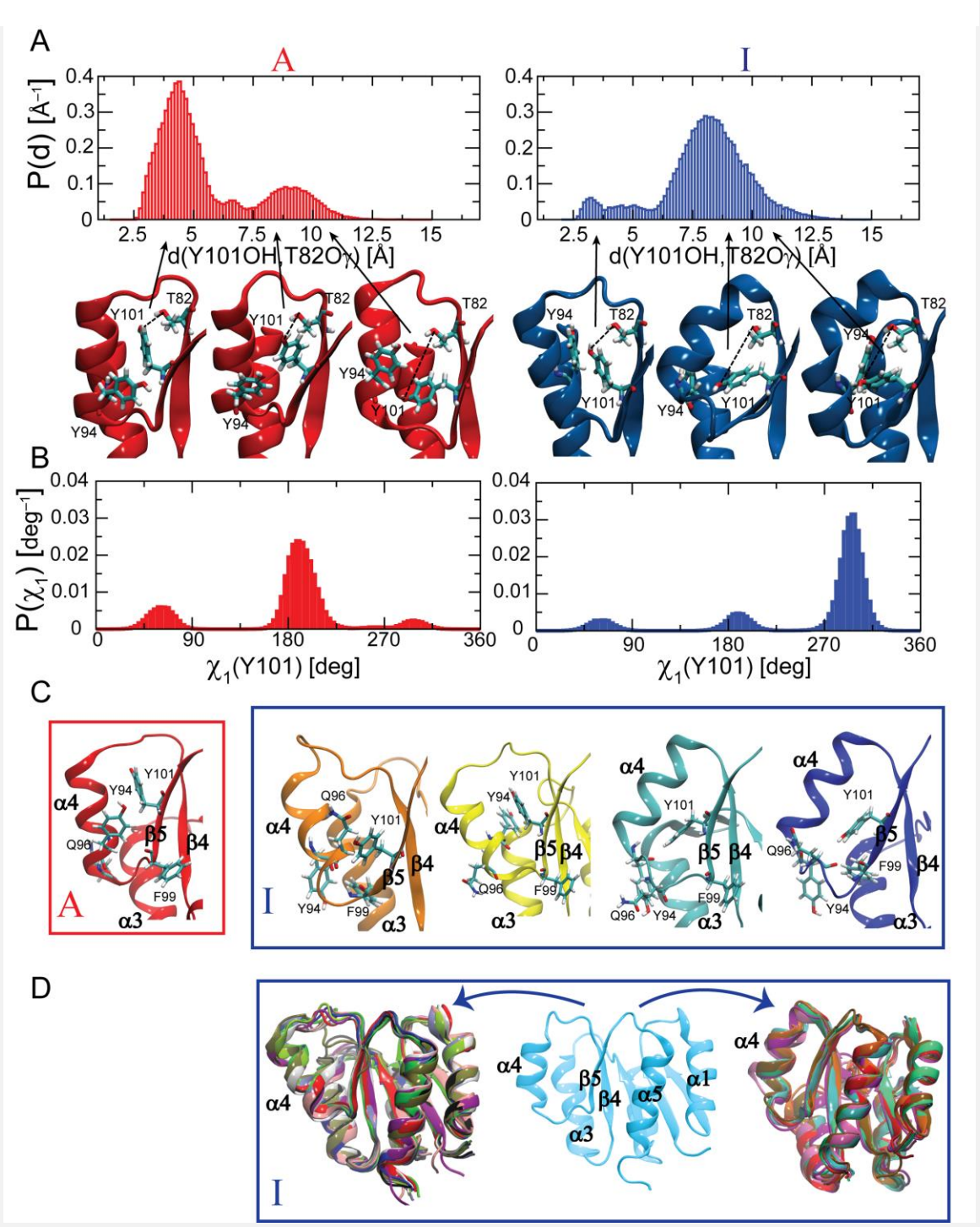

Supplementary Figure 3: Additional analysis on active and inactive macro-states from the MSM analysis.

A) The direct interaction between T82 and Y101 is not stable in the active state. The same direct interaction is observed in both the inactive and active macrostates in the MSM, though with different probability distributions. Moreover, in both the active and inactive states, tyrosine Y101 can sample all three rotameric states irrespective of the position of T82 (shown in selected structural snapshots). **B)** Distributions of the χ_1 dihedral angle of Y101 sampled in the two

macrostates. **C)** Some of the most different arrangements of the helix α4 sampled in the inactive macrostate are shown in the right panel. The orientation and secondary structural content of the helix α4 for some of these conformers are remarkably similar to the active state, shown in the left panel in red as a reference. While Y94 is oriented facing helix α3 in all the inactive conformers, other important side-chains can attain different conformations, suggesting that their rearrangement is not rate limiting and not fully correlated to the global active-inactive conformational transition. **D)** Some of the trajectories simulated on the F@H initiated from the same starting configuration fully commit to different inactive conformers with similar probability depicted in panel **C**, suggesting that these conformers are not high energy states along the inactive – active transition pathway, but represent sub-states with comparable free energy within the inactive macrostate.

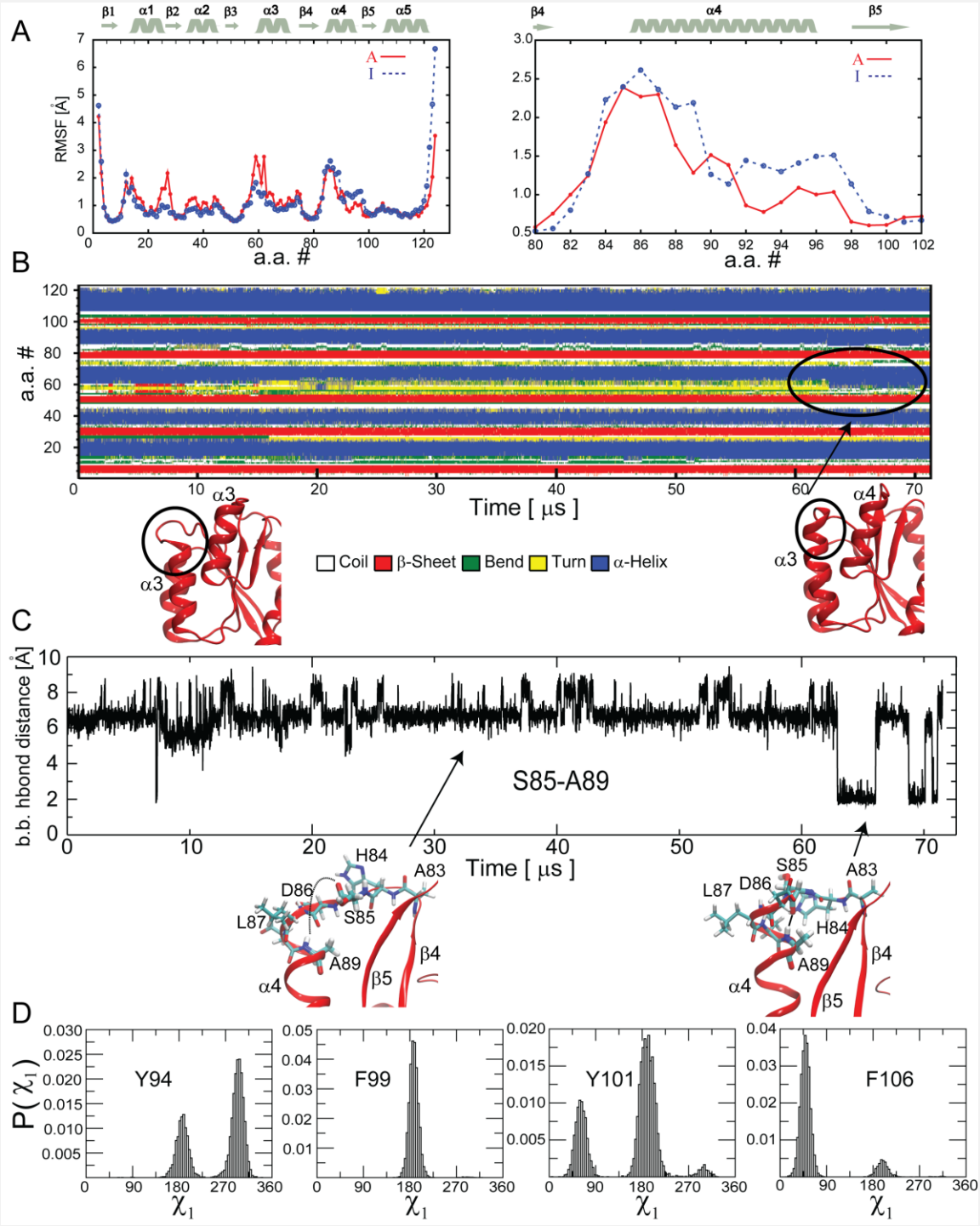

Supplementary Figure 4: Fluctuations in the multi-microsecond long Anton MD trajectories.

A) Root mean square fluctuations (RMSF) measured along the ~21μs MD simulation started from the inactive state model (blue), and along the ~71μs performed in the active state model (red). **B)** In the active state simulation, the fluctuations at the N-terminus of helix α3 result in an extension of 1 turn of the helix, which seems stable for at least the last 10μs of the simulation. This

suggests either an imperfection of the initial structure used, that is corrected by the MD sampling, or might instead point at imperfections in the force field used, which in long simulation might accumulate, favoring non-native structures. Similar phenomena were already observed elsewhere [6, 7] and recently prompted the development of an improved version of the CHARMM force field, unfortunately not available at the time that our calculations were performed. **C)** Fluctuation of the distance between backbone NH of A89 and CO of S85. Although the magnitude of the fluctuations in the N-terminus of helix $\alpha 4$ is similar to those observed in the simulation of the inactive state, these fluctuations do not reflect a global change of the conformation of the helix. The secondary structure of the helix remains stable throughout the simulation, except for the last 10μs, where attempts to form an extra turn in the N-terminus are observed. These excursions into high-energy states do not result in a full transition to the inactive basin. **D)** Distribution of the χ_1 dihedral angles of some aromatic side-chains during the active state simulations. The timescale associated with changes in side-chain rotameric states can be vastly different. Some of these side-chains experience rapid fluctuations among all the three different available isomeric states, while F99 stays in a single conformation for the whole duration of the simulation.

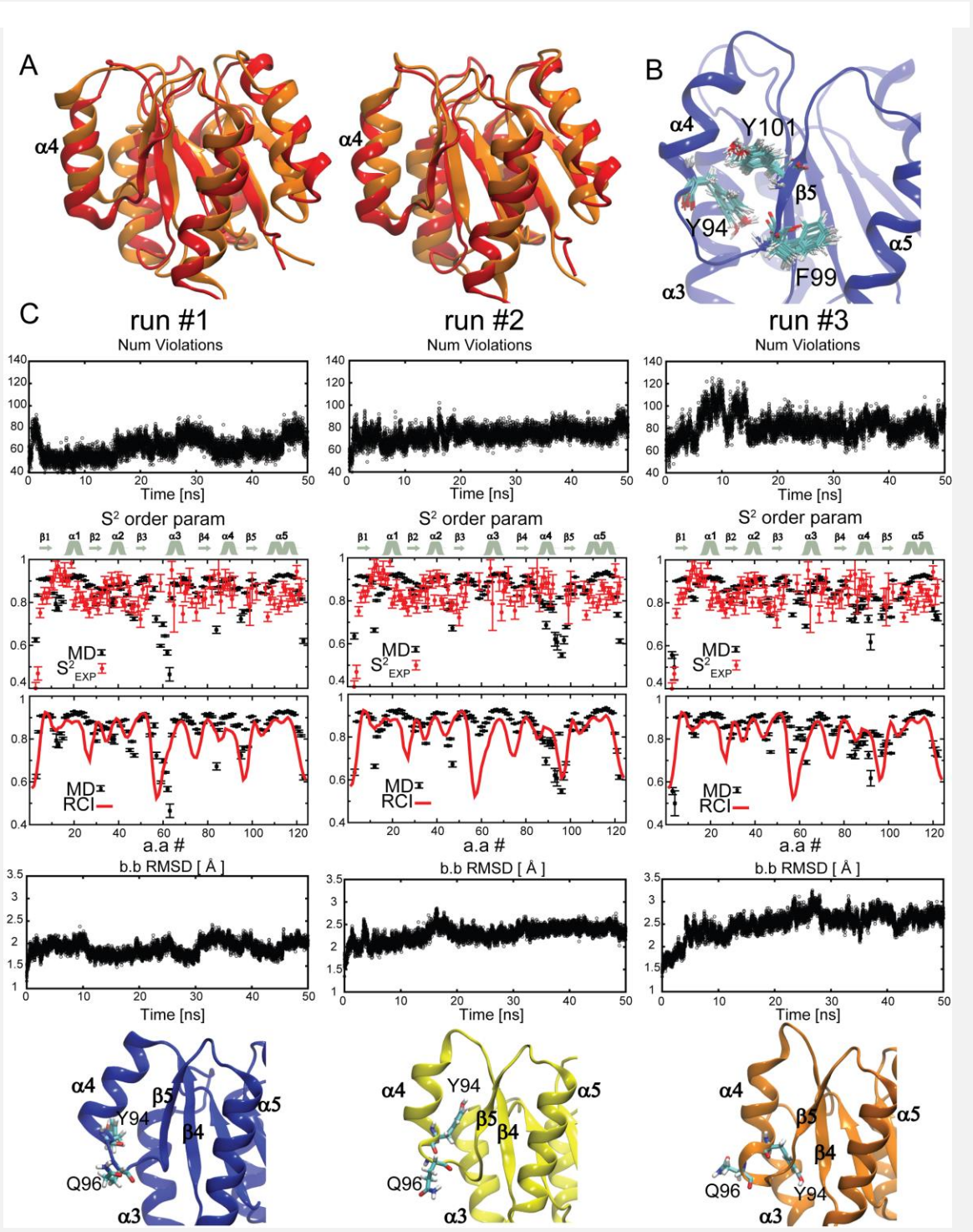

Supplementary Figure 5: Molecular Dynamics equilibration of the new NMR structures.
A) Superposition of the new NMR structure of the active conformation (red) and the model used for the simulation of the active state (orange). The tilt of the helix observed in the new refined structure appears slightly different from the initial active state model used for the simulations (left). However, within a few μs the simulations sample configurations extremely close to the new NMR model (right). **B)** Contrary to the previously available model, in the new NMR structure of the inactive state, F99 is facing helix α5. **C)** Some of the MD equilibrations of the new NMR

structural models of the apo state capture the heterogeneity observed in the previous computational results. For 3 equilibrations of new NMR models the following parameters are shown:
-The number of NOE violations computed along 50 ns of free simulations performed after releasing the experimental restraints (see methods);
-A comparison between the S^2 order parameters estimated from the last 30 ns of the simulations (black points) and the measured model free order parameters (red points) [8].
-A comparison between the S^2 order parameters estimated from the last 30 ns of the simulations (black points) and the S^2 order parameters estimated from the chemical shifts using the Random Coil Index, RCI (red lines) [9, 10, 11].
In both cases the error bars for the S^2 estimated from the simulation reflect the distribution of the values of the auto correlations of the amide bonds used to estimate the order parameter.
-Backbone RMSD.
-A cartoon representation of the arrangement of helix $\alpha 4$ in the sampled structure closest to the average structure of the last 30 ns of each trajectory. For reference, the side-chains of Y94 and Q96 are shown as licorice. The structures sampled recapitulate the heterogeneity observed in the MSM calculations.

Supplementary References:

1. Noe F, Horenko I, Schutte C, Smith JC. Hierarchical analysis of conformational dynamics in biomolecules: transition networks of metastable states. *J Chem Phys* **126**, 155102 (2007).

2. Deuflhard P, Weber M. Robust Perron cluster analysis in conformation dynamics. *Linear Algebra and its Applications* **398**, 161-184 (2005).

3. Schutte C, Fischer A, Huisinga W, Deuflhard P. A direct approach to conformational dynamics based on hybrid Monte Carlo. *J Comput Phys* **151**, 146-168 (1999).

4. Noe F, Schutte C, Vanden-Eijnden E, Reich L, Weikl TR. Constructing the equilibrium ensemble of folding pathways from short off-equilibrium simulations. *P Natl Acad Sci USA* **106**, 19011-19016 (2009).

5. Prinz JH*, et al.* Markov models of molecular kinetics: Generation and validation. *J Chem Phys* **134**, (2011).

6. Best RB, Buchete NV, Hummer G. Are current molecular dynamics force fields too helical? *Biophys J* **95**, L7-L9 (2008).

7. Best RB, Hummer G. Optimized Molecular Dynamics Force Fields Applied to the Helix-Coil Transition of Polypeptides. *J Phys Chem B* **113**, 9004-9015 (2009).

8. Volkman BF, Lipson D, Wemmer DE, Kern D. Two-state allosteric behavior in a single-domain signaling protein. *Science* **291**, 2429-2433 (2001).

9. Berjanskii M, Wishart DS. NMR: prediction of protein flexibility. *Nature protocols* **1**, 683-688 (2006).

10. Berjanskii MV, Wishart DS. The RCI server: rapid and accurate calculation of protein flexibility using chemical shifts. *Nucleic acids research* **35**, W531-537 (2007).

11. Berjanskii MV, Wishart DS. A simple method to predict protein flexibility using secondary chemical shifts. *Journal of the American Chemical Society* **127**, 14970-14971 (2005).